3D Stochastic Geometry Model for Aerial Vehicle-Relayed Ground-Air-Satellite Connectivity

Yulei Wang*†, Yalin Liu†, Yaru Fu†, Yujie Qin‡, and Zhongjie Li*
*College of Electronics and Information Engineering, South-Central Minzu University, Wuhan 430074, China
†School of Science and Technology, Hong Kong Metropolitan University,Hong Kong 999077, China
‡School of Information and Communication Engineering, University of Electronic Science and Technology of China, Chengdu 610054, China
Email: {ylwang, lizhongjie}@mail.scuec.edu.cn, {ylliu, yfu}@hkmu.edu.hk, yujie.qin@kaust.edu.sa

***Abstract*—Due to their flexibility, aerial vehicles (AVs), such as unmanned aerial vehicles and airships, are widely employed as relays to assist communications between massive ground users (GUs) and satellites, forming an AV-relayed ground-air-satellite solution (GASS). In GASS, the deployment of AVs is crucial to ensure overall performance from GUs to satellites. This paper develops a stochastic geometry-based analytical model for GASS under Matérn hard-core point process (MHCPP) distributed AVs. The 3D distributions of AVs and GUs are modeled by considering their locations on spherical surfaces in the presence of high-altitude satellites. Accordingly, we derive an overall connectivity analytical model for GASS, which includes the average performance of AV-relayed two-hop transmissions. Extensive numerical results validate the accuracy of the connectivity model and provide essential insights for configuring AV deployments.**

***Index Terms*—Matérn hard-core point process (MHCPP), ground-air-satellite solution (GASS), 3D stochastic geometry.**

I. Introduction

With the proliferation of communication satellites, such as Starlink [1], future wireless networks are expected to provide seamless coverage for global-range applications, including remote sensing, navigation, disaster management, and other commercial uses [2]. However, due to their long-range propagation, satellites cannot support stable connections with ground users (GUs) [2]. To address this issue, various emerging aerial vehicles (AVs), such as unmanned aerial vehicles and airships, can be employed as aerial relays to facilitate communication between GUs and satellites. This *AV-relayed ground-air-satellite solution (GASS)* is crucial to support data uploading of massive GUs for diverse Internet of Things tasks in the future [3]. In GASS, the deployment of AVs is essential to ensure overall performance from GUs to satellites. Particularly, multiple AVs can be widely deployed to cover massive GUs. In addition, global-range AVs can relay data to satellites to reduce the access burden from massive GU.

To investigate the deployment of AVs, previous studies modeled their distributions as stochastic point processes and analyzed transmission performance among AVs, GUs, and satellites [4]–[9]. Specifically, studies in [4], [5] modeled AVs' distribution using a homogeneous Poisson point process (HPPP) for air-ground communications and air-satellite networks, respectively. However, due to the independent nature of HPPP, random point locations in an HPPP can overlapp, it cannot cater to the practical distribution of multiple AVs, i.e., any two AVs should maintain a certain distance to avoid collisions. To address this issue, the authors in [6], [7] adopted

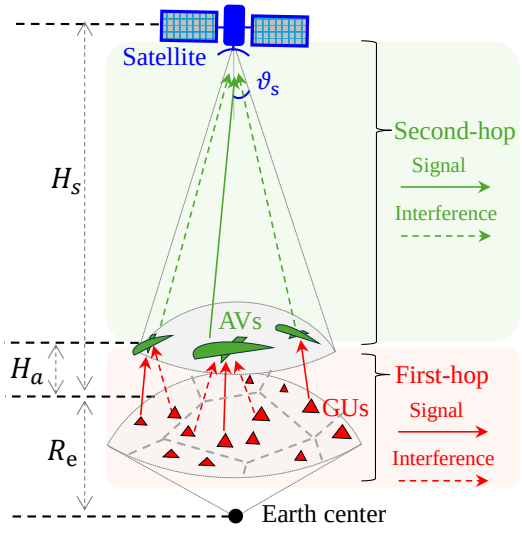

Fig. 1: A typical AV-relayed two-hop transmission scenario in GASS. Herein R_e is the earth radius, H_s and H_a are the height of satellites and AVs over the ground, respectively.

the Matérn hard-core point process (MHCPP) to model AVs' locations by introducing a minimum distance between all AVs. However, they considered the MHCPP in a plane, whereas AVs in GASS should be distributed on a 3D surface above the ground in the presence of satellites. Taking the 3D distribution into account, the works in [8], [9] explore the 3D location modeling of AVs. Nevertheless, [8] mainly investigated air-satellite performance without considering the coverage of GUs. Although [9] examined the AV-relayed performance from GUs to satellites, the AVs were still modeled using an HPPP. In summary, there is a lack of performance analysis work for GASS in consideration of precise 3D MHCPP distributions for AVs.

To fill in the above research gap, we aim to develop a stochastic geometry-based analytical model for GASS under 3D MHCPP-distributed AVs. However, this aim faces several challenges. First, there is no prior modeling of 3D locations for MHCPP-distributed AVs. Second, exploring the geometric relationships among AVs, served GUs, and satellites is inherently complex. Finally, considering the various transmission links among AVs, GUs, and satellites in GASS, constructing an analytical performance model is particularly challenging. To

address these challenges, we explore the spherical coverage regions of satellites and AVs and model the 3D locations of AVs and GUs in the regions. Accordingly, we investigate the overall performance of GASS by finding the average transmission performance of all possible links. Overall, our key contributions are summarized as follows:

- We develop a 3D node distribution model of GASS. In the presence of high-altitude satellites, the 3D distributions of AVs and GUs are modeled by considering their locations on spherical surfaces. Catering to practical node deployments, GUs are associated with their nearest AVs; the latter is distributed as an MHCPP.
- We present a stochastic geometry-based analytical model for GASS. This model derives the overall connectivity for typical AV-relayed two-hop transmissions in GASS. Based on stochastic geometry, the average transmission performance of each hop is analyzed by considering all possible links from distributed transmitters of that hop.
- We conduct extensive numerical analyses for the overall connectivity analytical model. The simulation results validate the accuracy of the model and provide essential insights for practical practitioners, e.g., configuring AV deployments to enhance performance in GASS.

The remainder of the paper is organized as follows. Section II introduces the system model. The 3D spherical geometry-based analytical model is presented in Section III. Section IV gives the numerical results. Section V concludes this paper.

II. System Model

A. Network Model

We consider a typical AV-relayed two-hop transmission scenario in GASS. As shown in Fig. 1, a reference satellite accepts the data from multiple AVs that serve as relay nodes collecting data from numerous GUs. Multiple AVs hover at a height H_a to cover ground regions. In practice, the two neighboring AVs generally maintain a distance from each other to avoid collisions and ensure efficient coverage. In this case, we use an MHCPP of type II (called MHCPP for short) Φ_a[1] to model the distribution of AVs and ensure a minimum distance $\check{d}$ among any two AVs. Φ_a is generated by thinning an original HPPP Φ_a^0. Let λ_a^0 be the node density in Φ_a^0 and $p_a\left(\check{d}\right)$ be the probability of retaining an AV in Φ_a^0. $p_a\left(\check{d}\right)$ is given by [11]

$$p_a\left(\check{d}\right)=\begin{cases}\frac{1-\exp\left(-\lambda_a^0\pi\check{d}^2\right)}{\lambda_a^0\pi\check{d}^2} & \check{d}>0\\ 1 & \check{d}=0\end{cases}. \tag{1}$$

After the thinning, Φ_a has the node density $\lambda_a=\lambda_a^0 p_a\left(\check{d}\right)$. The GUs are uniformly scattered on the Earth's surface (i.e., ground). Hence, we model the location distribution of GUs as an HPPP Φ_u with density λ_u. Each GU associates with its geographically nearest AV for transmission, where a Voronoi tessellation of Φ_u according to multiple AVs is formed [12]. Meanwhile, each GU is considered to have data to transmit to its associated AV with the probability p_u^t. Using the thinning process of HPPP, the transmitting GUs form an independent HPPP Φ_u^t ($\Phi_u^t\subset\Phi_u$) with density $\lambda_u^t=p_u^t\lambda_u$. In the presence of satellites, the 3D locations of AVs and GUs are modeled based on a spherical surface, as presented in Section III-A.

[1]We choose MHCPP of type II because it results in a higher density of effective points than MHCPP of type I for any density and hardcore [10].

B. Transmission Model

The two-hop transmission in GASS includes: i) the first-hop link from a reference GU to its associated AV, and ii) the second-hop link from the AV to a reference satellite. For convenience, the subscript $i, i\in\{1,2\}$ is adopted to indicate the first link and the second link, respectively. Let G_i denote the receiver antenna gain of the i-th hop link. Its value is given by $G_i=\iota_i\left(\pi D_i f_i/c\right)^2$, where ι_i is the antenna illumination coefficient, f_i is the carrier frequency used, D_i is the diameter of the normalized reflector antenna, and c is the light speed [9]. For both links $i\in\{1,2\}$, line-of-sight (LoS) propagation dominates the small-scale fading process. We use Nakagami-m fading to capture the channel fading characteristics. Let h_i be the channel power gain of the i-th hop link, its probability density function (PDF) is given by $\frac{m_i^{m_i}}{\Gamma(m_i)\Omega_i^{m_i}}h_i^{m_i-1}\exp\left(-\frac{m_i}{\Omega_i}h_i\right)$ [13], where m_i is the shape parameter, Ω_i is the spread parameter, and $\Gamma(\cdot)$ is the standard gamma function [14]. Let $r_i(\mathtt{t})$ be the distance between the transmitter $\mathtt{t}$ and its receiver in the i-th hop link, the corresponding path loss $L_i(\mathtt{t})$ is given by [15]

$$L_i(\mathtt{t})=l_i\left(\frac{c}{4\pi f_i}\right)^2\left(r_i(\mathtt{t})\right)^{-2}, \tag{2}$$

where l_i is the additional loss caused by atmospheric effects and rain/fog attenuation.

C. Interference Model

Generally, frequency division multiple access technology is adopted to enable simultaneous transmissions from multiple transmitters (i.e., GUs and AVs) in each hop. However, the available carriers are limited compared to the number of transmitters under the wide coverage of GASS. Each link suffers interference when multiple transmitters choose the same carrier to transmit. To evaluate the link quality, the signal-to-interference-plus-noise ratio (SINR) at the receiver is measured. Let $\mathtt{SINR}_i$ be the SINR of the i-th hop link from a transmitter $\mathtt{t}_0$ to its receiver, which is given by

$$\mathtt{SINR}_i=\frac{P_iG_ih_iL_i(\mathtt{t}_0)}{I_i+W_i}, \tag{3}$$

where P_i is the transmission power of transmitters in the i-th hop link and $I_i=\sum_{\mathtt{t}\in\Phi_i'}P_iG_ih_iL_i(\mathtt{t})$ is the aggregated power of interfering signals at the receiver, where $\Phi_i'=\Phi_i\setminus\{\mathtt{t}_0\}$ is the set of interfering transmitters with $\Phi_1=\Phi_u^t, \Phi_2=\tilde{\Phi}_a$. W_i is an additive white Gaussian noise.

III. 3D Stochastic Geometry Model

This section analyzes the two-hop transmission performance in GASS, which is greatly affected by the interference in two-hop links. To characterize the interference, we first model the 3D distance distributions among GUs, AVs, and satellites for each hop. Based on stochastic geometry of 3D node distributions, we investigate the overall connectivity of GASS.

A. 3D Distribution Model

Let $\mathcal{A}_i (i \in \{1,2\})$ be the coverage region of a receiver for its transmitters in the i-th hop link. The ground is approximated as a spherical surface with the Earth center $\mathbf{O}$. Given all transmitters at the same altitude, $\mathcal{A}_i$ can be approximated as a spherical cap. For the i-th hop link, all transmitters under the same receiver have the potential to transmit their data. Due to the distribution of transmitters, the distances $r_i(\mathtt{t})$ from different transmitters $\mathtt{t}$ to the same receiver are different. Below, we evaluate the distribution of $r_i(\mathtt{t})$ for two-hop links.

1) $\mathcal{A}_1$ and $r_1(\mathtt{t})$: For the first hop link, given a reference AV, $\mathcal{A}_1$ is the AV's coverage for GUs and $r_1(\mathtt{t})$ is the distance between the AV and any one of GUs $\mathtt{t}$ under its coverage. All AVs are generally configured with adaptive antennas to serve GUs dynamically from all directions [16]. Recall that the GUs and their associated AVs form a Voronoi tessellation; the associated coverage of each AV forms a Voronoi cell. The mean area of these Voronoi cells is given by $1/\lambda_a$ [12], which can be approximated to a spherical cap $\mathcal{A}_1$. Referring to Archimedes' hat theorem, the cap $\mathcal{A}_1$'s height H_1 is given by $H_1 = |\mathcal{A}_1|/(2\pi R_{\mathrm{e}}) = 1/(2\pi\lambda_a R_{\mathrm{e}})$. According to the geometry relationship in Fig. 1, the minimum and maximum distances of $r_1(\mathtt{t})$ are given by $\check{R}_1, \hat{R}_1$ as follows.

$$\check{R}_1 = H_a, \hat{R}_1 = \sqrt{H_a^2 + 2H_1\left(R_{\mathrm{e}} + H_a\right)}. \tag{4}$$

Since the GUs follow an HPPP, the PDF $f(r_1)$ of $r_1(\mathtt{t})$ on $\mathcal{A}_1$ can be derived by

$$f(r_1) = \frac{\mathrm{d}\frac{|\mathcal{A}_1(r_1)|}{|\mathcal{A}_1(\hat{R}_1)|}}{\mathrm{d}r_1} = \frac{\frac{\pi\lambda_a R_{\mathrm{e}}\left(r_1^2 - \check{R}_1^2\right)}{\left(R_{\mathrm{e}} + \check{R}_1\right)}}{\mathrm{d}r_1} = \frac{2\pi\lambda_a R_{\mathrm{e}} r_1}{R_{\mathrm{e}} + \check{R}_1}. \tag{5}$$

2) $\mathcal{A}_2$ and $r_2(\mathtt{t})$: For the second hop link, given a reference satellite, $\mathcal{A}_2$ is the satellite's coverage for AVs and $r_2(\mathtt{t})$ is the distance between the satellite and any one of AVs $\mathtt{t}$ under its coverage. The satellite is considered to cover the earth surface vertically with its antenna. Let ϑ_s be the 3dB beamwidth of the satellite, which is given by $\vartheta_s = c\kappa_s/(f_2 D_2)(\text{degrees})$. Similar to (4), the minimum and maximum distances of $r_2(\mathtt{t})$ are given by $\check{R}_2, \hat{R}_2$ as follows.

$$\begin{aligned}\check{R}_2 = H_s - H_a, \hat{R}_2 = \left(R_{\mathrm{e}} + H_s\right)\cos\vartheta_s \\ - \sqrt{\left(R_{\mathrm{e}} + H_a\right)^2 - \left(R_{\mathrm{e}} + H_s\right)^2 \sin^2\vartheta_s}.\end{aligned} \tag{6}$$

Referring to Archimedes' hat theorem, the cap $\mathcal{A}_2$'s height and the area of $\mathcal{A}_2$ are given by $H_2 = (\hat{R}_2^2 - \check{R}_2^2)/(2\left(R_{\mathrm{e}} + H_s\right))$ and $|\mathcal{A}_2| = 2\pi\left(R_{\mathrm{e}} + H_a\right)H_2$, respectively. Recall that the AVs follow an MHCPP (type II) Φ_a. For interference analysis of multiple AVs, Φ_a can be approximated by an HPPP $\tilde{\Phi}_a$ with the same density λ_a, as validated in [10]. Therefore, we consider the approximate distribution $\tilde{\Phi}_a$ for AVs. Considering GUs $\tilde{\Phi}_a$, the PDF of $r_2(\mathtt{t})$ on $\mathcal{A}_2$ can be derived by

$$f(r_2) = \frac{\mathrm{d}\frac{r_2^2 - \check{R}_2^2}{\hat{R}_2^2 - \check{R}_2^2}}{\mathrm{d}r_2} = \frac{2r_2}{\hat{R}_2^2 - \check{R}_2^2}. \tag{7}$$

B. Overall Connectivity Model

We investigate the overall connectivity of two-hop transmissions in GASS by including the average successful probability (ASP) of two-hop transmissions. Based on the stochastic geometry, the ASP of each hop is evaluated as the average transmission performance of all possible links in that hop. Let $\overline{\mathcal{P}}_{\mathrm{overall}}, \overline{\mathcal{P}}_i (i \in \{1,2\})$ be the overall connectivity and ASPs of two-hop links. The performance $\overline{\mathcal{P}}_{\mathrm{overall}}$ is evaluated by

$$\overline{\mathcal{P}}_{\mathrm{overall}} \triangleq \prod_{i\in\{1,2\}} \overline{\mathcal{P}}_i, \overline{\mathcal{P}}_i = \int_{\check{R}_i}^{\hat{R}_i} \mathcal{P}_i f\left(r_i\right) \mathrm{d}r_i, \tag{8}$$

where $\mathcal{P}_i$ is the conditional successful probability of a particular i-th hop link. $\mathcal{P}_i$ represents the probability of the signal from the transmitter to the receiver being successfully received and decoded, i.e., the SINR measured at the receiver exceeds a certain threshold. Let θ_i be the SINR threshold of transmitters in the i-th hop link. $\mathcal{P}_i\left(\theta_i\right)$ is given by

$$\mathcal{P}_i \triangleq \mathbb{P}\left(\mathtt{SINR}_i > \theta_i | \Phi_i\right). \tag{9}$$

Substituting Eq. (3) into (9), we have Proposition 1.

Proposition 1. *$\forall i \in \{1,2\}$, $\mathcal{P}_i$ is given by*

$$\begin{aligned}&\mathcal{P}_i = \exp\left(-\dot{S}_i - \dot{R}_i\varepsilon_i\right) \\ &\times \sum_{k=0}^{m_i-1}\sum_{l,q,k}\left[\frac{1}{i!j!...q!}\left(\dot{S}_i + \dot{R}_i\varepsilon_i'\right)^i\left(\dot{R}_i\varepsilon_i''\right)^j ... \left(\dot{R}_i\varepsilon_i^{(l)}\right)^q\right], \\ &\text{where } \dot{S}_i = \frac{16 m_i\theta_i\sigma_i^2(r_i(\mathtt{t}_0))^2}{\Omega_i P_i \iota_i l_i \mathrm{D}_i^2}, \dot{R}_i = \left\{\frac{\pi\lambda_i R_{\mathrm{e}}}{R_{\mathrm{e}}+H_a}, \frac{\pi\lambda_i(R_{\mathrm{e}}+H_a)}{R_{\mathrm{e}}+H_s}\right\}, \\ &\varepsilon_i = \int_{\check{R}_i^2}^{\hat{R}_i^2}\left(1 - \left(1 + \frac{\theta_i(r_i(\mathtt{t}_0))^2}{\gamma}\right)^{-m_i}\right)\mathrm{d}\gamma, \gamma = (r_i(\mathtt{t}))^2, \\ &\varepsilon_i^{(l)} = C_l^{m_i+l-1}\int_{\check{R}_i^2}^{\hat{R}_i^2}\left(\frac{\theta_i(r_i(\mathtt{t}_0))^2}{\gamma}\right)^l\left(1 + \frac{\theta_i(r_i(\mathtt{t}_0))^2}{\gamma}\right)^{-m_i-l}\mathrm{d}\gamma, \\ &\lambda_i = \{p_u^t\lambda_u, \lambda_a^0 p_a\left(\check{d}\right)\}, \check{R}_i = \{H_a, H_s - H_a\}, \\ &\text{and } \hat{R}_i = \{\sqrt{H_a^2 + 2H_1\left(R_{\mathrm{e}} + H_a\right)}, \left(R_{\mathrm{e}} + H_s\right)\cos\vartheta_s - \\ &\sqrt{\left(R_{\mathrm{e}} + H_a\right)^2 - \left(R_{\mathrm{e}} + H_s\right)^2\sin^2\vartheta_s}\}.\end{aligned}$$

Proof: The proof is given in Appendix A. ■

Remarks: Substituting Proposition 1 into (8), we can calculate $\overline{\mathcal{P}}_{\mathrm{overall}}$. Referring to Proposition 1 and (8), it can be seen that our analytical model can be used to investigate the effect of comprehensive system parameters, including two-hop topology settings $\{H_a, H_s, R_{\mathrm{e}}\}$, transceiver configurations $\{P_i, f_i, p_u^t, \iota_i, D_i, \kappa_s, \theta_i, r_i(\mathtt{t}_0)\}$, distribution parameters $\{\lambda_u, \lambda_a^0, \check{d}\}$, and channel factors $\{m_i, \Omega_i, l_i\}$. To analyze the impact of these parameters on our model, we conduct extensive numerical results in Section IV. Due to the length limit, several significant parameters $\{\check{d}, \lambda_a^0, \lambda_u, \theta_1, \theta_2\}$ are analyzed.

IV. Numerical Results

This section presents the numerical results of three metrics $\overline{\mathcal{P}}_1, \overline{\mathcal{P}}_2, \overline{\mathcal{P}}_{\mathrm{overall}}$ as given in Secion III. The parameter settings are set aligned with our previous work [9]. We conduct Monte Carlo simulations and take the average results over a total of 10^4 iterations. In each simulation, the random distributions of

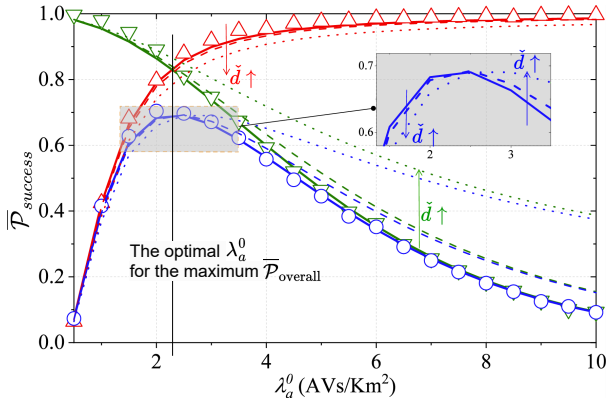

(a) λ_u = 50GUs/Km^2, θ_1 = 0dB, θ_2 = -5dB.

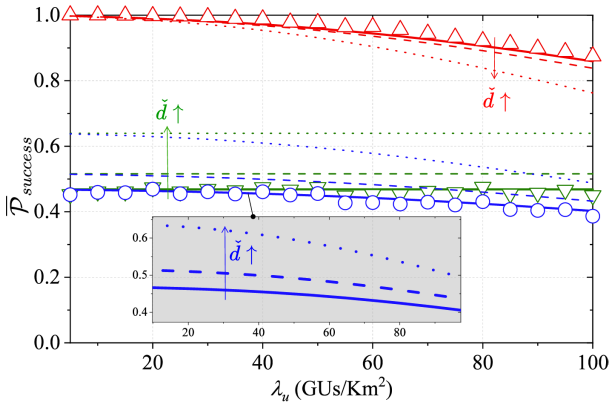

(b) λ_a^0 = 5AVs/Km^2, θ_1 = 0dB, θ_2 = -5dB.

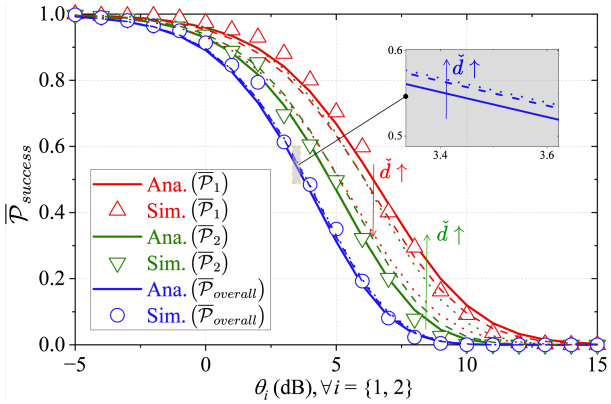

(c) λ_a^0 = 5AVs/Km^2, λ_u = 50GUs/Km^2

Fig. 2: Three metrics of $\overline{\mathcal{P}}_{success}$: $\overline{\mathcal{P}}_1, \overline{\mathcal{P}}_2, \overline{\mathcal{P}}_{\text{overall}}$ versus different parameters $\{\check{d}, \lambda_a^0, \lambda_u, \theta_1, \theta_2\}$, where H_s = 600Km, H_a = 1Km, $\{m_1, m_2\} = \{3, 3\}$, and $\{\Omega_1, \Omega_2\} = \{1, 1\}$. The "solid", "dash", and "dot" lines show the theoretical results under $\check{d} = \{0, 100, 200\}$m respectively. The simulation results under $\check{d} = \{100, 200\}$m are not shown to avoid overlapping.

GUs and AVs as well as the random channel fading of both links are generated. In our resulting Fig. 2, the labels "Ana." and "Sim." represent the theoretical and simulation results, respectively. Besides, one legend remains for all subfigures to ensure clarity of the plotted results and avoid overlapping.

Fig. 2(a) shows the impact of $\lambda_a^0, \check{d}$ on $\overline{\mathcal{P}}_1, \overline{\mathcal{P}}_2, \overline{\mathcal{P}}_{\text{overall}}$. We can see that the increasing λ_a^0 leads to the increasing $\overline{\mathcal{P}}_1$ and decreasing $\overline{\mathcal{P}}_2$; the larger $\check{d}$ leads to the smaller $\overline{\mathcal{P}}_1$ and the larger $\overline{\mathcal{P}}_2$. This is because a larger λ_a^0 means more relays (i.e, AVs), thus reducing the coverage burden of each AV and enhancing $\overline{\mathcal{P}}_1$. More AVs also introduce greater interference in the second hop, then lowering $\overline{\mathcal{P}}_2$. Meanwhile, the larger $\check{d}$ can reduce the AVs density, thus increasing the coverage burden of each AV and decreasing $\overline{\mathcal{P}}_1$. In contrast, fewer AVs lead to smaller interference, thus enhancing $\overline{\mathcal{P}}_2$. As a result, the overall performance $\overline{\mathcal{P}}_{\text{overall}}$ can be enhanced under careful settings of λ_a^0 and $\check{d}$: i) given a $\check{d}$, an optimal value of λ_a^0, denoted by λ_a^* (when $\overline{\mathcal{P}}_1 = \overline{\mathcal{P}}_2$), can be used for the maximum $\overline{\mathcal{P}}_{\text{overall}}$; ii) given $\lambda_a^0 < \lambda_a^*$, the smaller $\check{d}$ can enhance $\overline{\mathcal{P}}_{\text{overall}}$; and iii) given $\lambda_a^0 > \lambda_a^*$, the larger $\check{d}$ can enhance $\overline{\mathcal{P}}_{\text{overall}}$.

Fig. 2(b)-(c) show the impact of $\lambda_u, \theta_i (\forall i = \{1, 2\}), \check{d}$ on $\overline{\mathcal{P}}_1, \overline{\mathcal{P}}_2, \overline{\mathcal{P}}_{\text{overall}}$. It is observed that the increasing λ_u reduces $\overline{\mathcal{P}}_1, \overline{\mathcal{P}}_{\text{overall}}$ while it doesn't affect $\overline{\mathcal{P}}_2$; the increasing θ_i results in a decrease of $\overline{\mathcal{P}}_1, \overline{\mathcal{P}}_2, \overline{\mathcal{P}}_{\text{overall}}$. This is because a larger λ_u means more GUs, bringing more interference in first-hop transmissions, thereby reducing $\overline{\mathcal{P}}_1$. The second hop performance $\overline{\mathcal{P}}_2$ is related to the AV relays, then it won't be affected by λ_u. In summary, as λ_u increases, $\overline{\mathcal{P}}_2$ decreases, and $\overline{\mathcal{P}}_2$ stay unchanged, then $\overline{\mathcal{P}}_{\text{overall}}$ decreases. Meanwhile, a larger θ_i increases the difficulties of decoding signals in two-hop links, thus lowering $\overline{\mathcal{P}}_1, \overline{\mathcal{P}}_2$ and $\overline{\mathcal{P}}_{\text{overall}}$. In Fig. 2(b)-(c), $\overline{\mathcal{P}}_{\text{overall}}$ increases with the growth of $\check{d}$. This is due to the relatively large value of $\lambda_a^0 > \lambda_a^*$, as we observed in Fig. 2(a).

Overall, all simulation results closely align with the theoretical ones, validating the accuracy of our analytical model. Meanwhile, our observations offer essential insights for practitioners, such as network operators or engineers, in finding the optimal parameter settings to enhance system performance. For example, the observations in Fig. 2(a) can assist in configuring AVs' deployments, including λ_a^0 and $\check{d}$, and then enhancing the overall two-hop transmission performance.

V. Conclusion

This paper presents an overall connectivity analytical model to characterize the average performance of two-hop transmissions in GASS. Specifically, we use HPPP and MHCPP to model the location distributions of GUs and AVs. We explore the distribution of GUs associated with AVs and model the spherical locations of AVs to reflect practical network deployment. By applying stochastic geometry tools, we derive mathematical expressions for the spherical distance distributions of the two-hop transmission links, as well as ASPs and the overall connectivity for these links. Extensive Monte Carlo simulations have been conducted, and the results validate the accuracy of the proposed analytical model.

VI. Acknowledgment

The work of this paper was fully supported by the Hong Kong UGC/FDS project under reference No. UGC/FDS16/E15/24. This work of Yulei Wang was completed when he was at Hong Kong Metropolitan University.

APPENDIX

The proof of Proposition 1:

$$\mathcal{P}_i = \mathbb{P}\left(\frac{P_i G_i h_i L_i(\mathtt{t}_0)}{I_i+\sigma_i^2} > \theta_i \middle| \Phi_i\right) = 1 - \mathbb{P}\left(h_i \le \frac{\theta_i\left(I_i+\sigma_i^2\right)}{P_i G_i L_i(\mathtt{t}_0)} \middle| \Phi_i\right)$$
$$\overset{(a)}{=} 1 - \mathbb{E}_{I_i}\left[\frac{\gamma\left(m_i, \frac{m_i\theta_i\left(I_i+\sigma_i^2\right)}{\Omega_i P_i G_i L_i(\mathtt{t}_0)}\right)}{\Gamma(m_i)}\right] \overset{(b)}{=} \mathbb{E}_{I_i}\left[\frac{\Gamma\left(m_i, s_i\left(I_i+\sigma_i^2\right)\right)}{\Gamma(m_i)}\right]$$
$$\overset{(c)}{=} \mathbb{E}_{I_i}\left[\exp\left(-s_i\left(I_i+\sigma_i^2\right)\right)\sum_{k=0}^{m_i-1}\frac{\left(s_i\left(I_i+\sigma_i^2\right)\right)^k}{k!}\right]$$
$$\overset{(d)}{=} \sum_{k=0}^{m_i-1}\frac{\left(-s_i\right)^k}{k!}\mathbb{E}_{I_i}\left[\frac{\mathrm{d}^k \exp\left(-s_i\left(I_i+\sigma_i^2\right)\right)}{\mathrm{d}s_i^k}\right]$$
$$= \sum_{k=0}^{m_i-1}\frac{\left(-s_i\right)^k}{k!}\left[\exp\left(-s_i\sigma_i^2\right)\mathcal{L}_{I_i}\left(s_i\right)\right]_{s_i}^{(k)}, \tag{10}$$

where $s_i = m_i\theta_i/(\Omega_i P_i G_i L_i(\mathtt{t}_0))$. (a) arises from the cumulative distribution function of the gamma-distributed h_i. (b) comes from the substitution of $\Gamma(s) = \gamma(s,x) + \Gamma(s,x)$, where $\gamma(s,x)$ and $\Gamma(s,x)$ are the lower and upper incomplete gamma function, respectively. (c) is resulted from the incomplete gamma function [17, 8.352.2]. (d) arises from the substitution of $\exp(-sx)\,x^k = (-1)^k\frac{\mathrm{d}^k\exp(-sx)}{\mathrm{d}s^k}$ [18]. In (10), $\mathcal{L}_{I_i}(s_i)$ is the Laplace transform of the interference I_i, which can be further calculated by

$$\mathcal{L}_{I_i}\left(s_i\right) = \mathbb{E}_{I_i}\left[\exp\left(-s_i I_i\right)\right]$$
$$\overset{(a)}{=} \mathbb{E}_{r_i(\mathtt{t})}\left[\mathbb{E}_{h_i}\left[\exp\left(-\sum_{\mathtt{t}\in\Phi_i'} s_i P_i G_i h_i L_i(\mathtt{t})\right)\right]\right]$$
$$\overset{(b)}{=} \mathbb{E}_{r_i(\mathtt{t})}\left[\prod_{\mathtt{t}\in\Phi_i'}\mathbb{E}_{h_i}\left(\exp\left(-s_i P_i G_i L_i(\mathtt{t}) h_i\right)\right)\right]$$
$$\overset{(c)}{=} \mathbb{E}_{r_i(\mathtt{t})}\left[\prod_{\mathtt{t}\in\Phi_i'}\left(1+s_i Q_i L_i(\mathtt{t})\right)^{-m_i}\right], \tag{11}$$

where $Q_i = P_i G_i \Omega_i/(m_i)$. (a) comes from the fact that $r_i(\mathtt{t})$ and h_i are mutually independent. (b) follows from the property of exponential distribution, i.e., $\exp\left(\sum_j h_i\right) = \prod_j \exp(h_i)$. (c) comes from the moment-generating function of h_i [19]. According to the probability generating functional of an HPPP, i.e., $\mathbb{E}\left[\prod_{x\in\Phi} f(x)\right] = \exp\left(-\lambda\int_{\mathbb{R}^d}(1-f(x))\,\mathrm{d}x\right)$, Eq. (11) can be calculated by

$$\mathcal{L}_{I_i}\left(s_i\right) \overset{(a)}{=} \exp\left(-\lambda_i\int_{\mathcal{A}_i}\left(1-\left(1+s_i Q_i L_i(\mathtt{t})\right)^{-m_i}\right)\mathrm{d}\mathtt{t}\right)$$
$$\overset{(b)}{=} \exp\left(-\lambda_i\int_0^{2\pi}\int_0^{\varphi_{\mathtt{t}}}\int_{\check{R}}^{\hat{R}}\left(1-\left(1+s_i Q_i L_i(\mathtt{t})\right)^{-m_i}\right) r^2\sin\varphi\mathrm{d}r\mathrm{d}\varphi\mathrm{d}\vartheta\right)$$
$$\overset{(c)}{=} \exp\left(-2\pi\lambda_i\tilde{R}_{\mathrm{e}}^2\int_0^{\varphi_{\mathtt{t}}}\left(1-\left(1+s_i Q_i L_i(\mathtt{t})\right)^{-m_i}\right)\sin\varphi\mathrm{d}\varphi\right). \tag{12}$$

In (12), (a) comes from the integral of the interfering GU (or AV) $\mathtt{t}$ in $\mathcal{A}_i$. (b) is resulted from the conversion from Cartesian coordinates $\mathtt{t}:(x,y,z)$ to polar coordinates $\mathtt{t}:(r,\varphi,\vartheta)$, i.e., $\mathrm{d}\mathtt{t} = \mathrm{d}x\mathrm{d}y\mathrm{d}z = r^2\sin\varphi\mathrm{d}r\mathrm{d}\varphi\mathrm{d}\vartheta$, $r\in[\check{R},\hat{R}]$ is the radial distance, $\vartheta\in[0,2\pi]$ is the azimuthal angle, $\varphi\in[0,\varphi_{\mathtt{t}}]$ is the polar angle. In (c), $\check{R} = \hat{R} = \tilde{R}_{\mathrm{e}}$. Because the GUs/AVs located on the spherical surface with radius $\tilde{R}_{\mathrm{e}}$, and

$$\tilde{R}_{\mathrm{e}} = \begin{cases} R_{\mathrm{e}}, & i=1 \\ R_{\mathrm{e}}+H_a, & i=2 \end{cases}.$$

Substituting (12) into (10) and following the similar derivation process in [9], we have Proposition 1. ■

REFERENCES

[1] X. Luo, H.-H. Chen, and Q. Guo, "LEO/VLEO satellite communications in 6G and beyond networks–technologies, applications and challenges," *IEEE Netw.*, 2024.

[2] A. Talgat, M. A. Kishk, and M.-S. Alouini, "Maximizing uplink data transmission of LEO satellite-based wireless-powered IoT," *IEEE Internet of Things Journal*, vol. 11, no. 17, pp. 28 975–28 987, 2024.

[3] Y. Fu, Y. Shan, Q. Zhu, K. Hung, Y. Wu, and T. Q. Quek, "A distributed microservice-aware paradigm for 6G: Challenges, principles, and research opportunities," *IEEE Netw.*, vol. 38, no. 3, pp. 163–170, 2023.

[4] Y. Qin, M. A. Kishk, and M.-S. Alouini, "On the downlink SINR meta distribution of UAV-assisted wireless networks," *IEEE Trans. Commun.*, vol. 71, no. 11, pp. 6762–6778, 2023.

[5] Y. Liu, H.-N. Dai, and N. Zhang, "Connectivity analysis of UAV-to-satellite communications in non-terrestrial networks," in *2021 IEEE Global Communications Conference (GLOBECOM)*. IEEE, 2021, pp. 1–6.

[6] S. Zhang, Y. Zhu, and J. Liu, "Multi-UAV Enabled Aerial-Ground Integrated Networks: A Stochastic Geometry Analysis," *IEEE Trans. Commun.*, vol. 70, no. 10, pp. 7040–7054, 2022.

[7] W.-Y. Dong, S. Yang, P. Zhang, and S. Chen, "Stochastic geometry based modeling and analysis of uplink cooperative satellite-aerial-terrestrial networks for nomadic communications with weak satellite coverage," *IEEE J. Sel. Areas Commun.*, vol. 42, no. 12, pp. 3428–3444, 2024.

[8] Y. Tian, G. Pan, M. A. Kishk, and M.-S. Alouini, "Stochastic analysis of cooperative satellite-UAV communications," *IEEE Wirel. Commun.*, vol. 21, no. 6, pp. 3570–3586, 2022.

[9] Y. Liu, H.-N. Dai, Q. Wang, O. J. Pandey, Y. Fu, N. Zhang, D. Niyato, and C. C. Lee, "Space-air-ground integrated networks: Spherical stochastic geometry-based uplink connectivity analysis," *IEEE J. Sel. Areas Commun.*, vol. 42, no. 5, pp. 1387–1402, 2024.

[10] M. Haenggi, "Mean interference in hard-core wireless networks," *IEEE Commun. Lett.*, vol. 15, no. 8, pp. 792–794, 2011.

[11] Y. Wang, Q. Zhao, S. Yao, M. Zhou, L. Feng, and P. Zhang, "Analytical modeling of location and contention randomness for node-assisted WiFi backscatter communication," *IEEE Internet Things J.*, vol. 11, no. 13, pp. 23 336–23 347, July 2024.

[12] Y. Wang, L. Feng, S. Yao, H. Liang, H. Shi, and Y. Chen, "Outage probability analysis for D2D-enabled heterogeneous cellular networks with exclusion zone: A stochastic geometry approach," *CMES-Computer Modeling in Engineering & Sciences*, vol. 138, no. 1, pp. 639–661, 2024.

[13] Z. Song, J. An, G. Pan, S. Wang, H. Zhang, Y. Chen, and M.-S. Alouini, "Cooperative satellite-aerial-terrestrial systems: A stochastic geometry model," *IEEE Trans. Wirel. Commun.*, vol. 22, no. 1, pp. 220–236, 2022.

[14] B. Sklar, *Digital communications: fundamentals and applications*. Pearson, 2021.

[15] D.-H. Jung, J.-G. Ryu, W.-J. Byun, and J. Choi, "Performance analysis of satellite communication system under the shadowed-rician fading: A stochastic geometry approach," *IEEE Trans. Commun.*, vol. 70, no. 4, pp. 2707–2721, 2022.

[16] A. I. Alshbatat and L. Dong, "Performance analysis of mobile ad hoc unmanned aerial vehicle communication networks with directional antennas," *International Journal of Aerospace Engineering*, vol. 2010, no. 1, p. 874586, 2010.

[17] I. S. Gradshteyn and I. M. Ryzhik, *Table of integrals, series, and products*. Academic press, 2014.

[18] B. Galkin, J. Kibiłda, and L. A. DaSilva, "A stochastic model for UAV networks positioned above demand hotspots in urban environments," *IEEE Trans. Veh. Technol.*, vol. 68, no. 7, pp. 6985–6996, 2019.

[19] M. K. Simon and M.-S. Alouini, *Digital communication over fading channels*. John Wiley & Sons, 2004, vol. 86.